Article

Study on the Influence of Groundwater Variation on the Bearing Capacity of Sandy Shallow Foundation

Wenfeng Chen [1,2], Weishu Xia [1], Shanshan Zhang [1] and Erlei Wang [3,*]

1 School of Civil Engineering and Architecture, Wuhan University of Technology, 122 Luoshi Rd., Wuhan 430070, China
2 Changjiang Institute of Survey, Planning, Design and Research Co., Ltd., Wuhan 430010, China
3 Design & Research Institute of Wuhan University of Technology, Wuhan 430070, China
* Correspondence: wangerlei@whut.edu.cn

Abstract: Groundwater variation has a significant effect on the bearing capacity of sandy shallow foundations. Groundwater and capillary water in the shallow foundation would result in the various water distributions in the soil mass. Therefore, there are three types of water conditions in the shallow foundation. They are the total saturated, capillary-water-effect zone and dry soil. In this study, a physical mode experimental was developed to investigate the effect of groundwater variation on the deformation behavior under different loading conditions. The effect of water level and fluctuation times were examined by a novel setup with a water-pressure control system. A total of 10 group model tests were carried out. The results indicated that the relationship between water level height and foundation bearing capacity is negatively correlated. In addition, the numerical analysis was carried out to investigate the effect of water-level change on the bearing capacity of the foundation. The bearing capacity of the foundation decreases as the water-level cycles increase. The increase in the fluctuation range of the water level will decrease the bearing capacity of the foundation. The outcome of this study would be helpful to predict the bearing capacity of shallow foundations due to the change of the water level.

Keywords: sandy soil; bearing capacity; numerical analysis; water-level change

1. Introduction

Buildings in cities along rivers or coastal lines are often accompanied by the problem of foundation submergence during design, construction and use [1,2]. Rivers or oceans can raise the water table of coastal foundations to a certain extent. The engineering properties of naturally deposited coarse-grained soils (such as gravel layer, pebble, gravelly soil and medium coarse-grained sand) have little change in their natural or saturated state. Fine-grained soils (such as fine sand, silt and clay) are quite different. Their mechanical properties will change if saturated, and the shear strength will be reduced to different degrees, and this is not conducive to the safety and stability of the foundation [3–6]. At present, the engineering community usually regards "capillary rise height plus foundation burial depth" as the standard of the critical depth of submergence of buildings without fully considering the rise of the water table on the physical and mechanical properties of the foundation soil layer [7]. The evaluation of building submergence according to this criterion is imperfect, and sometimes there are certain risks. Therefore, it is necessary to conduct an in-depth study on the influence of the foundation's bearing capacity brought by the water-level change [8,9].

The bearing capacity of the foundation is an important index to evaluate the strength and stability of the foundation in the field of geotechnical engineering. The theoretical research related to the bearing capacity of foundations under general conditions has been relatively mature. Scientists such as Terzaghi, Hansen and Khalid [10–12] have proposed various methods to calculate the bearing capacity of soil. Terzaghi first proposed the

bearing-capacity equation, considering the general shear failure of soil under a rough strip foundation. Using the superposition principle, he demonstrated the influence of the cohesion of the soil, the angle of internal friction, the overload (soil at the foundation level), the unit weight of the soil and the width of the foundation on the ultimate bearing pressure. Later, Hansen introduced two factors, foundation shape and load angle, into the bearing-capacity equation. Khalid et al. studied the influence of foundation burial depth and groundwater level on the bearing capacity of rectangular foundations. They found that when the depth of the foundation increased, the bearing capacity increased too. Boushehrian and Hataf [13] conducted experimental and numerical studies on the bearing capacity of a model circular foundation which was on reinforced soils. Dixit and Patil [14] found that cohesion and internal friction angle are important parameters for determining soil bearing capacity. These scholars have constantly improved the calculation methods, which make it easy to calculate the foundation bearing capacity under general conditions. However, the formulas that they came up with cannot be directly applied to the calculation of foundation bearing capacity under the condition of groundwater-level fluctuation. The problem of fluid–solid interaction is not fully considered. Studies have shown that the coupling effect of water and soil has a certain impact on the bearing performance of soil and can be characterized by the model [15].

Due to the constant ebb and flow of the Yangtze River in China, the foundations of buildings along the coast remain under fluctuating water levels for a long time. The influence of the fluctuating water level on the foundation cannot be ignored, and it often leads to the softening of the foundation and a decrease in the bearing capacity [16,17]. Therefore, it is meaningful to study the influence of fluctuating water level on the bearing capacity of the foundation. However, the existing calculation methods of foundation bearing capacity cannot be directly applied to the situation of groundwater-level fluctuation, so it is necessary to study a more suitable method [18–21]. In this study, in view of the existing problems in the study of the influence of inundation on physical model tests, a bearing-capacity analysis was carried out. The sandy soil along the Yangtze River was used as the model foundation. The sand particles were fine, and the degree of saturation had an obvious influence on the engineering characteristics of the sand [22,23]. A self-made water pump was used to control the water level of the model foundation, and the hydraulic servo system was used to load the model foundation, so as to obtain the bearing capacity of the model foundation under different water levels. The form and mechanism of the influence of groundwater-level variation on the foundation bearing capacity were examined. The influence of saturation on the strength and deformation index of sandy soil was analyzed. By carrying out the numerical simulation of foundation finite element at different water-table heights, the effect of the soil water content on the foundation bearing capacity was calculated, and the reliability of the model was verified. Finally, numerical simulation was used to predict the changes in the foundation bearing capacity under different water-level changes. Effective measures to prevent the decline of the foundation bearing capacity were put forward, combined with practical projects to give early warning of disasters caused by the decline of the foundation bearing capacity [24–26]. The specific research process is shown in Figure 1.
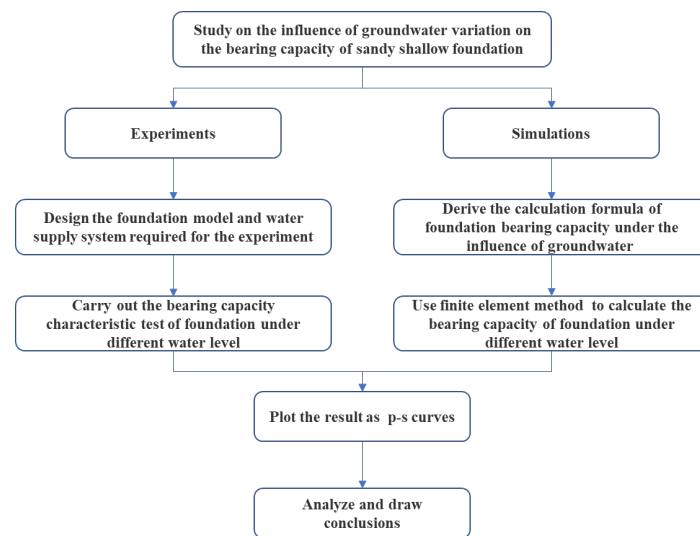
Figure 1. Flowchart of the overall research.

2. Experimental Tests

2.1. Materials

The sandy soils used in the tests were taken from the foundations along the Yangtze River. This kind of sand has fine particles. The degree of saturation has an obvious influence on the engineering characteristics. Their relevant material properties are shown in Table 1 [27,28].

Table 1. Related parameters of test soil.

Parameter / Soil Sample	Density, ρ (g/cm^3)	Cohesive Force, c (kPa)	Angle of Internal Friction, φ (°)	Young's Modulus, E (MPa)	Poisson's Ratio, M
Silty sand (natural)	1.92	12.7	20.1	15.0	0.25
Silty sand (saturated)	2.05	8.4	18.3	9.4	0.25
Gravel	2.20	3.2	38.7	150	0.3

2.2. Experimental Setup

In order to investigate the effect of water-level change on the foundation bearing capacity, the model box foundation bearing capacity test was carried out. In Figure 2, the experimental equipment is shown, which includes a transparent glass model box, a pneumatic control system, a water pump, a loading system, a PIV shooting system and a data-acquisition system. The purposes of each section are as follows:

(a) The model box with transparent glass: Its purpose is to hold the foundation soil. It has an inlet at the bottom to let water in and out. The size of the model box is 1.2 m × 0.6 m × 0.6 m. The bottom of the model is covered with 0.1 m gravel, and the layer above is 0.35 m thick. The water level in the soil can be seen through clear glass because saturated soil is darker than unsaturated soil. The glass is marked with a scale to measure the height from the bottom of the model box to the water level.

(b) Air-pressure control system: It controls the air pressure in the pump to move water in and out of the model box

(c) Water pump: Its purpose is to simulate groundwater.

(d) Loading system. It can apply vertical load to the foundation soil through the loading plate. The loads can be controlled by the loading system.

(e) PIV filming system: It can capture the displacements of foundation soil by using PIV technology.

(f) Data-acquisition system: It shows the displacement change captured by PIV through the color change of the image, so that the final displacement can be calculated.

Figure 2. Model box test equipment.

2.3. Experiment Program

This test is mainly performed to study the influence of the water-level height change and times of water-level cycle on the bearing capacity of the foundation. The times of water-level cycle refers to the number of cycles between the water level rising to the specified height and falling to the bottom of the model box. There are 10 groups in this test. The maximum elevation of the water surface is determined by the capacity of the pump, and the times of cycles are controlled by the working mode of the air compressor. Specific test conditions are shown in Table 2.

Table 2. Test conditions.

Number	Factors	Hight of Water Level (mm)	Times of Water-Level Cycle
1		0	0
2		50	1
3		50	15
4		50	30
5		100	1
6		100	15
7		100	30
8		150	1
9		150	15
10		150	30

2.4. Test Procedures

The whole test includes the following five steps:

1. First, lay the gravel blocks into the model box and spread a layer of permeable cloth on the gravel blocks to prevent the upper sand from falling into the gravel blocks. Adjust the water level to soak the gravel blocks [29]. Next, put sandy soil into the model box and compact it.

2. Turn on the air-pressure control system and increase the air pressure to raise the water level to the specified height. Then control the air pressure to lower the water level to the initial level and repeat for the specified number of times.

3.   After the cycle is completed, start the loading system to pressurize the foundation. Use the PIV system to photograph the settlement and deformation of the foundation in time [30,31].
4.   When the foundation is damaged, stop loading. Record the pressure and save the photos of the PIV shooting system.
5.   Finally, remove and dry the foundation soil for the next set of tests.

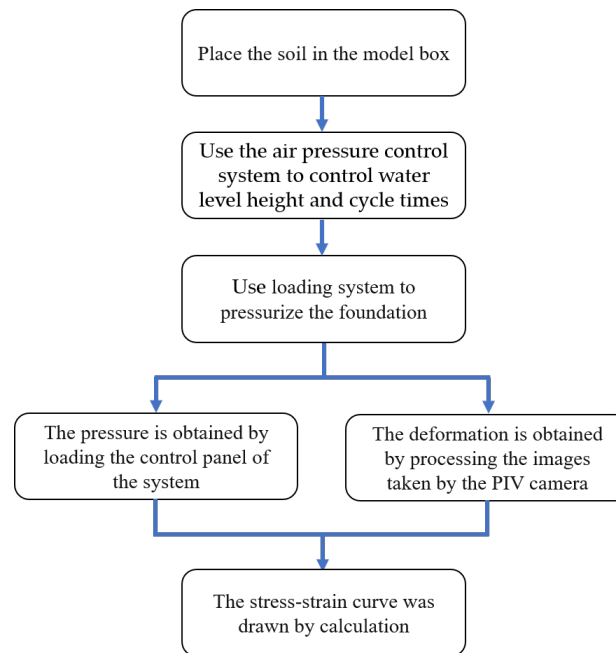The flowchart of the experiment is shown in Figure 3.

Figure 3. The flowchart of the experiment.

2.5. Analysis of Results

The data-processing results of the tests are shown in Figures 4 and 5. In the figure, p represents the upper pressure, and s represents the displacement of the loading plate.
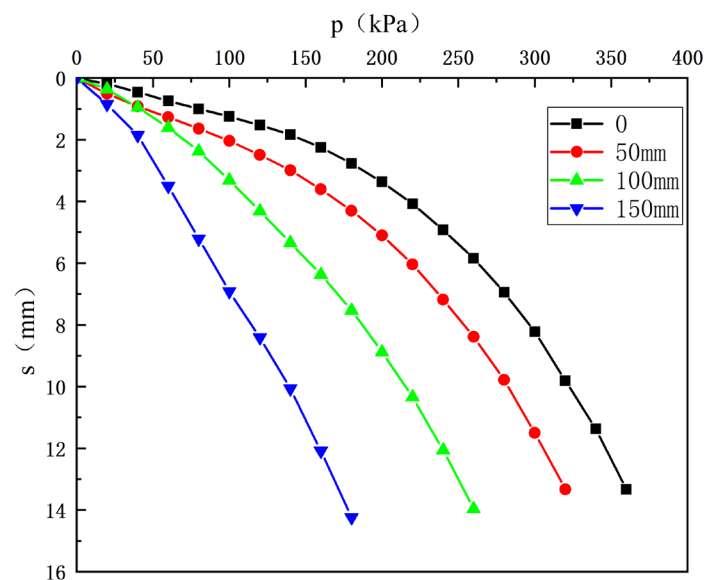

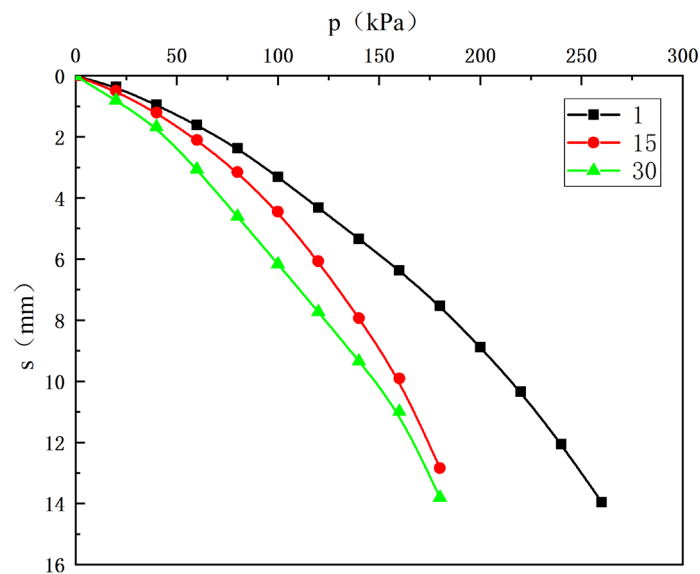**Figure 4.** The p–s curves at different water levels.

Figure 5. The p–s curves under different cycles.

When the number of cycles is the same and the water level rises gradually from 0 to 50 mm, 100 mm and 150 mm, the foundation bearing capacity gradually drops from 360 kPa to 320 kPa, 260 kPa and 180 kPa, with a decrease of 11.1%, 18.8% and 30.8%, respectively. It indicates that the foundation bearing capacity decreased with the rise of the water level. With the gradual rise of the water level, the changes in the percentage of the foundation bearing capacity also increased. The increase in the water level improved the soil moisture content affected by water level, and the increase in the soil moisture content reduced the soil cohesion and internal friction angle. These are important factors that affect the bearing capacity of the foundation [32]. Specifically, the change of soil from an unsaturated state to a saturated state improved its plasticity. This makes it easier for the soil with a high degree of saturation to change from elastic to plastic under the same upper load, thus reducing the bearing capacity of the foundation. The rise in the water level is a process of increasing soil saturation, thus softening the soil and reducing the carrying capacity. When the water level was low, the bearing capacity of the foundation did not decrease significantly, because most of the soil in the soil was still in the unsaturated state and the shear strength was relatively high. However, when the water level increased, the soil-saturation degree increased. The bearing capacity of the foundation decreased obviously, and the softening of the foundation intensified.

The bearing capacity of the foundation decreased from 260 kPa to 180 kPa, with a decrease of 30.8%, as the water level was the same, and the number of cycles increased from 1 to 15 times. The bearing capacity of the foundation decreased from 180 kPa to 170 kPa, with a decrease of 5.6%, as the number of cycles increased from 15 to 30 times. This indicates that the foundation bearing capacity decreased with the increase in the water-level cycle times, because the water-level cycle changed the soil moisture content successively. With the increase in the water-level cycle times, the soil moisture content increased, resulting in the decrease in soil cohesion and internal friction angle. With the increase in the number of cycles, the reduction of the bearing capacity became smaller. The reason is that, with the increase in the number of cycles, the proportion of saturated soil continued to increase. Eventually, the soil was fully saturated, and the bearing capacity did not decrease any more.

3. Numerical Analysis

3.1. Numerical Model

COMSOL Multiphysics is based on the finite-element method. Through solving partial differential equations (single field) or partial differential equations (multi-field) to achieve

the simulation of real physical phenomena, it uses mathematical methods to solve the physical phenomena of the real world. It is good at solving the problem of multi-physical field coupling and can edit partial differential equations. As this problem is a fluid–structure coupling problem between water and soil, COMSOL can simulate this problem well.

The Darcy seepage water storage model was adopted as the model, and the governing equation is as follows:

$$\rho S \frac{\partial p}{\partial t} + \nabla \rho \left[-\frac{k}{\rho g} \left(-\frac{k}{\rho g} (\nabla p + \rho g \nabla D) \right) \right] = Q_m \tag{1}$$

In the formula, p is fluid pressure, and ρ is the fluid density between the pores of the porous medium. In this study, ρ is the density of water. S and k represent the water storage coefficient and the permeability coefficient, respectively. Q_m represents the mass source term. When there is no external flow supply, $Q_m = 0$. ∇D represents a unit vector in the direction of gravity.

The Mohr–Coulomb law is a classical method that is used to study the strength of soil. It is a formula of soil damage put forward by the French scientist Coulomb, who summarized the phenomenon and influencing factors of soil damage. The shear strength of soil depends on the properties of rock particles which are related to normal stress, internal friction angle and cohesion of soil [33–35]. Later, Mohr continued Coulomb's research and put forward the destruction of the material of shear failure theory. The function defined the Mohr failure envelope curve in the general case. The Mohr failure envelope can be expressed by the Coulomb formula, namely the soil shear strength and normal stress into linear function relation [36,37].

The constitutive relation that was selected for this model is Mohr–Coulomb criterion of rock failure because it is a classical theory in geotechnical engineering and has been widely verified. The Mohr–Coulomb constitutive relation requires fewer parameters and can reduce the error caused by finite element calculation.

For any stress surface considered in rock and soil under general stress conditions, its ultimate shear strength can usually be expressed by Coulomb's law:

$$\tau_n = \sigma_n \tan\varphi + c \tag{2}$$

In the spatial stress state, it can be expressed as follows:

$$\sigma_1 = \sigma_3 \tan^2 (45° + \frac{\varphi}{2}) + 2c\tan(45° + \frac{\varphi}{2}) \tag{3}$$

In the formula, σ is the shear strength index of the soil sand, and φ is the angle of the internal friction.

The above equation is the shear failure criterion of rock and soil. It can be called the failure yield surface equation [38]. The failure surface is the limit surface of the yield surface. Therefore, the yield surface can be expressed as follows:

$$F = -\frac{1}{3} I_1 \sin\varphi + \left(\cos\theta_\sigma - \frac{1}{3} \sin\theta_\sigma \sin\varphi \right) \sqrt{J_2} - c\cos\varphi = 0 \tag{4}$$

In the formula, $-\frac{\pi}{6} \leq \theta_\sigma \leq \frac{\pi}{6}$.

The problem is simplified as shown in Figure 6. The upper sandy soil is divided into three zones, which are Zones A, B and C. The sandy soil in Zone A is all unsaturated soil. Zone B is the mixed region of the saturated soil and unsaturated soil and contains the whole range of water level fluctuation. The sand soil in Zone C is saturated soil. The final problem is to determine the specific location and soil thickness of Zones A, B and C.

Among the three regions, Zone B is the most important, because it contains all the fluctuation of water level and is the key area to study the influence of water-level fluctuation on the foundation bearing capacity. The soil saturation in this region is very complex and is the most difficult part of this problem.
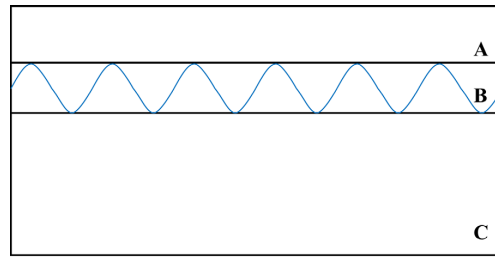
Figure 6. Simplified diagram of the problem.

The foundation problem with the dynamic change of groundwater level over a large area can be regarded as a one-dimensional problem, which can be directly described by the traditional consolidation governing equation:

$$Y(z)c_{vs}\frac{\partial^2 u}{\partial z^2} = \frac{\partial u}{\partial t} \tag{5}$$

In the formula, z represents the position variable along the depth of the soil layer, f is the time variable, u represents the excess pore pressure with depth z and time, and c_{vs} is the consolidation or rebound coefficient of the calculation model. In this paper, the possible changes of the foundation permeability coefficient and volume compression coefficient in the process of dynamic change of groundwater level are not taken into consideration temporarily. To simplify the calculation, c_{vs} is directly taken as the consolidation coefficient and a constant.

The mathematical expression of the dynamic change of groundwater head pressure over time is used to describe the top boundary conditions of the calculation model, which can be expressed as follows:

$$u|z = 0 = f(t) \tag{6}$$

The boundary condition of impervious boundary can be expressed as follows:

$$\frac{\partial u(H,t)}{\partial z} = 0 \tag{7}$$

In the formula, H is the total thickness of the model foundation.
The initial conditions are as follows:

$$u(z,0) = 0 \tag{8}$$

Assuming that the groundwater level presents regular harmonic changes, Equation (6) for the top pore pressure boundary condition of the calculation model can be expressed as follows:

$$u(0,t) = A\cos(\omega t) + B\sin(\omega t) \tag{9}$$

In the formula, A and B represent the variation amplitude of the harmonic component at the top pore pressure boundary, and ω is the angular frequency of change and the function relation of the period T is $\omega = 2\pi/T$.

According to the above boundary conditions and initial conditions, the analytical solution of excess pore pressure in the governing Equation (5) is solved by the Duhamel integral method:

$$u(z,t) = \int_0^t u(0,\tau)\frac{\partial \overline{u}(z,t-\tau)}{\partial t}d\tau \tag{10}$$

In the formula, the excess pore pressure in soil can be obtained by using the initial and boundary conditions.

3.2. Numerical Analysis Procedures

The two-dimensional model is similar in size to the indoor model box test, which aims to verify the reliability of the model by comparing the numerical simulation results with

the test results. Finally, it can predict the settlement of the foundation with the model and give an early warning for the foundation's safety. The specific steps of model establishment are as follows:

1. Establish a two-dimensional model. In order to improve the convergence of calculation, a symmetric structure was adopted with a length of 0.6 m and a width of 0.45 m. The soil was divided into two layers: gravel in the lower layer and sandy soil in the upper layer.
2. Input the material parameters of the soil which are shown in Table 1.
3. Set the boundary conditions of the model. The left side of the model is sliding support. The right side is a symmetric boundary. The lower side is a fixed constraint, and the right end of the upper side is the applied boundary load.
4. Add soil weight and pore water pressure. Set soil plasticity and enable Mohr–Coulomb strength criteria.
5. Add the global control equation. Use the parameter solver to control the gradual increase in load and define the integral function to record the vertical displacement of the loading midpoint.
6. Divide the finite element mesh. Use relatively dense mesh in the contact surface of two layers of soil and the fluctuation surface of the water level.
7. Calculate and output the stress and deformation and plastic development of the model and the p–s curves at the midpoint of loading.

3.3. Simulation Plan

For the simplification of the problem in Section 3.1, two influencing factors of water-level fluctuation range and water-level fluctuation form are added in the numerical simulation. The water-level fluctuation range refers to the thickness of Zone B in Section 3.1. The water-level distribution form contains the horizontal type, the simple harmonic type and the random function type. The specific simulated working conditions are shown in Table 3.

Table 3. Simulation of working conditions.

Number / Factors	Elevation of Water Level (mm)	Water-Level Fluctuation Range (mm)	Water-Level Fluctuation Form
1	50	10	sine wave
2	50	20	sine wave
3	50	30	sine wave
4	50	40	sine wave
5	100	10	sine wave
6	100	20	sine wave
7	100	30	sine wave
8	100	40	sine wave
9	150	10	sine wave
10	150	20	sine wave
11	150	30	sine wave
12	150	40	sine wave
13	50	30	straight line
14	100	30	straight line
15	150	30	straight line
16	50	30	random function
17	100	30	random function
18	150	30	random function

The water-level fluctuation form is shown in Figure 7. A straight line indicates no fluctuation in the water table. Sine waves represent fluctuations in water levels that are sinusoidal over time. The random function is a uniform distribution function.
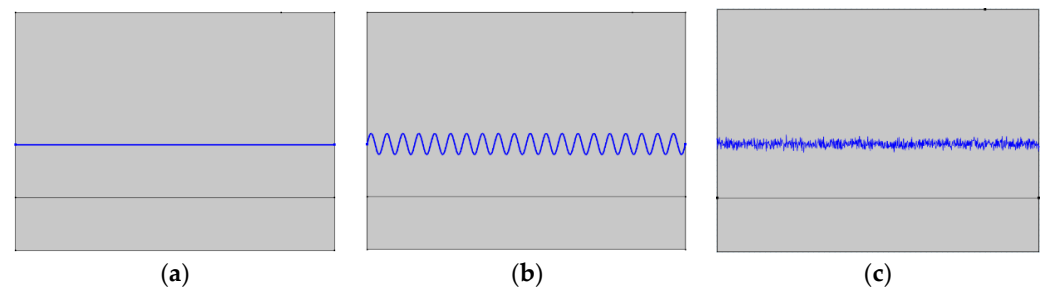
Figure 7. Schematic diagram of water level fluctuation form: (**a**) straight line, (**b**) sine wave and (**c**) random function.

As is shown in Figure 8, the stress and deformation of the foundation for the model under different upper loads assume that the water-level-fluctuation curve is sinusoidal. The closer the color is to red, the greater the stress in this region. The closer the color is to blue, the smaller the stress in this region. The vertical deformation in the upper right corner of the model represents the vertical settlement of the foundation soil under load. The stress and deformation of the soil increase under increasing upper loads, and the effect of the water-level fluctuation is also obvious. The foundation's settlement and the foundation's uplift around the loading can be clearly seen.

Figure 8. Variation of foundation stress and deformation with upper load.

Figure 9 shows the changes in the distribution of the foundation's plastic zone during the increasing upper load. The blue area represents the plastic deformation of the foundation soil. Due to the influence of gravity stress and pore water pressure on the lower part of the foundation, the plastic development degree of the lower part of the foundation is greater than that of the upper part of the foundation. It is obvious that the plastic zone develops continuously with the increasing upper load until it reaches the ultimate load.

Figure 10 is the control chart of the test results and numerical simulation results under different water-level heights. The average error of the experiment and simulation results is less than 8%. The error is within the acceptable range. The error is generated for the following reasons:

1. During the test, the water content of the soil layer above the water table increased due to the capillary phenomenon of the soil, which led to a decrease in the parameters of internal friction angle and cohesion and a decrease in the bearing capacity. The numerical simulation assumes that the water content of the soil above the water table is the initial water content. Therefore, the bearing capacity of the test result is smaller than that of the simulation result.

2.　The termination condition of loading during the test is according to the Geotechnical Test Procedure: the deformation of the foundation reaches 1/12 of the width of the loading plate. Then the foundation was considered to be damaged, and the loading was stopped. In contrast, the numerical simulation is loaded until the damage. Therefore, the test may not reach the ultimate bearing capacity of the foundation when the loading is stopped and the p–s curve has not reached the inflection point.
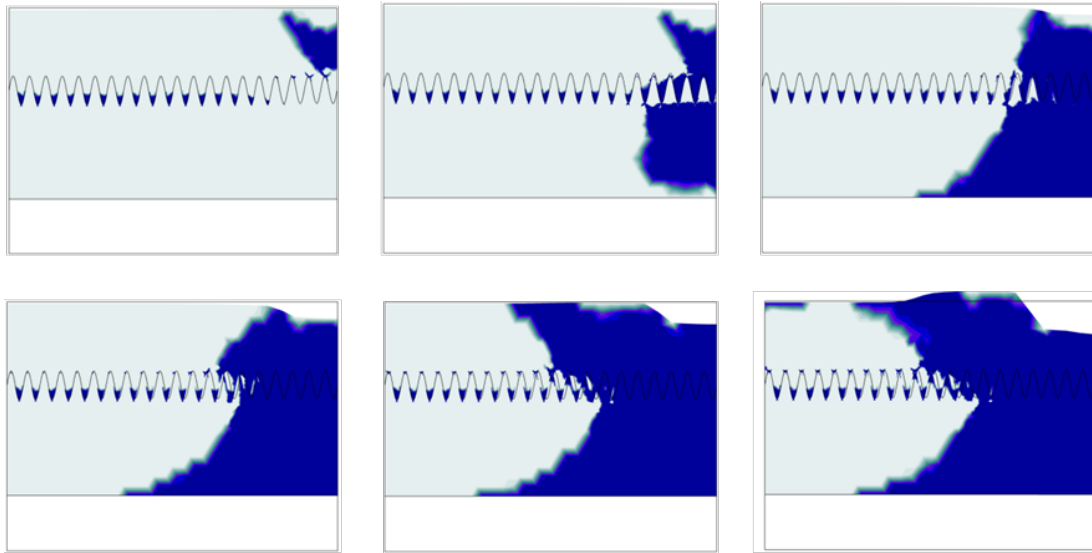

Figure 9. Variation of the distribution of the plastic zone of the foundation with the upper load.

Figure 10. Comparison of test and simulation results at different water-level heights: (**a**) initial water level, (**b**) 50 mm water level and (**c**) 100 mm water level.

3.4. Analysis of Simulation Results

Figure 11 is the p–s curve under different water-level fluctuation ranges. It can be concluded that, with the gradual increase in the fluctuation range, the foundation bearing capacity has a decreasing trend. This trend is in different water-level heights. When the water level height is 100 mm, the fluctuation range increases from 5 mm to 10 mm. The foundation bearing capacity decreases from 294.9 kPa to 287.8 kPa, and the decrease is 2.37%. The decrease is very small, which means that the fluctuation range brings less influence compared with the influence of the water-level height on the foundation bearing capacity. The main reason for the decrease in the bearing capacity is that the increase in fluctuation range will make the area affected by the water table line increase, and the water content of the upper soil layer will rise under the action of the capillary phenomenon, thus reducing the internal friction angle and cohesion of the soil and resulting in a decrease in the shear strength.
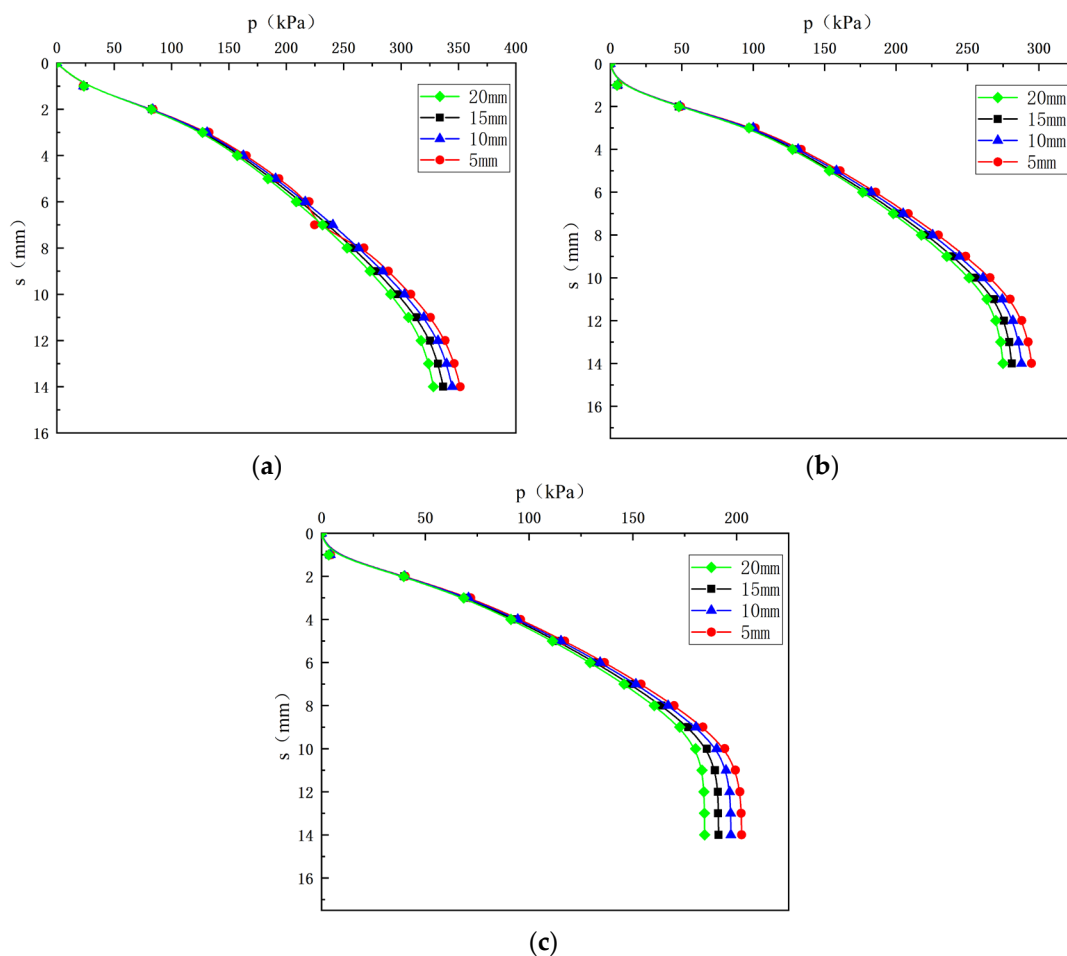

Figure 11. The p–s curves under different water level fluctuation ranges: (**a**) 50 mm water level, (**b**) 100 mm water level and (**c**) 150 mm water level.

The different water-level fluctuation form of the foundation load–displacement curve is shown in Figure 12. It can be found that different water-level fluctuation forms also influence the foundation bearing capacity. Specifically, the bearing capacity of foundation is larger under a linear water level, medium under a sinusoidal water level and smaller under random function distribution. The influence of the fluctuation form is also relatively small. The foundation bearing capacity is affected by the main reason that fluctuation makes the capillary phenomenon intensify. Water rises from below to above the groundwater level due to capillarity, which increases the saturation of the topsoil. The soil cohesion and

internal friction angle are reduced, and the shear strength is decreased. As the fluctuation frequency increases, the impact of the capillary phenomenon increases.
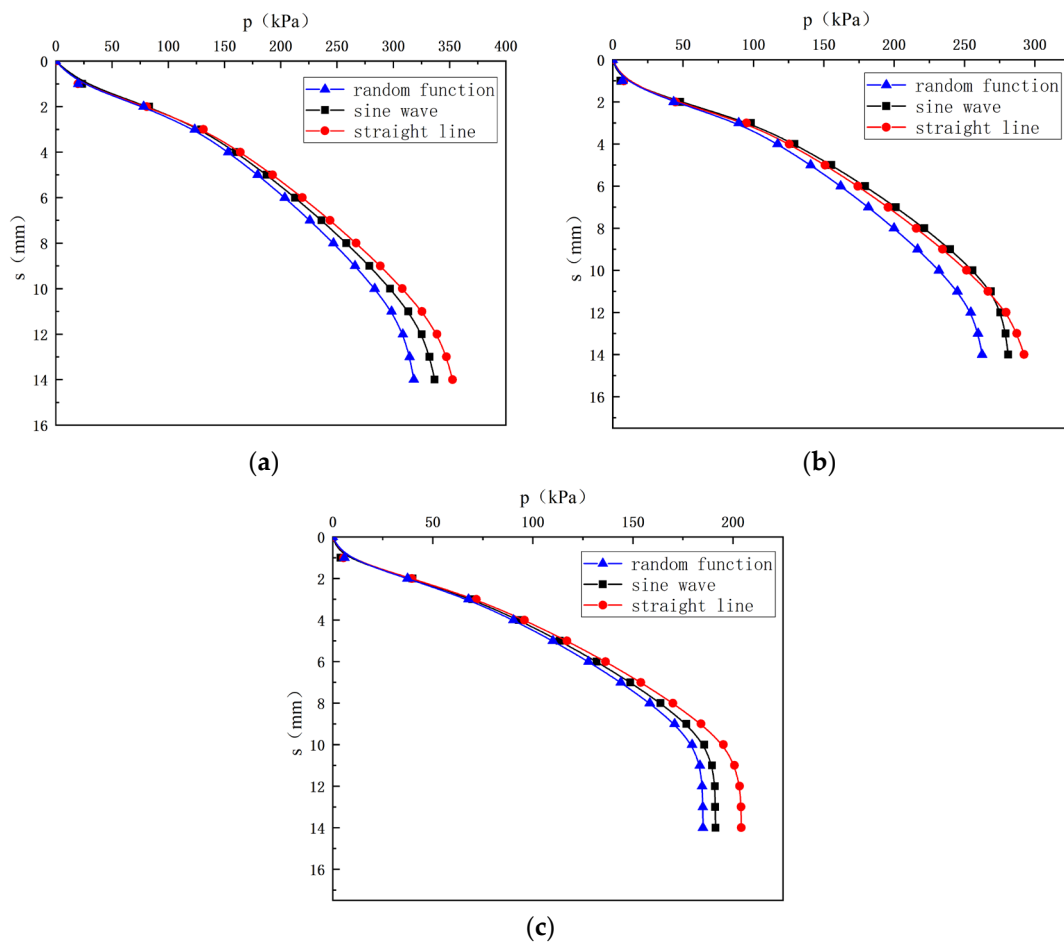

Figure 12. The p–s curves under different forms of water-level fluctuations: (**a**) 50 mm water level, (**b**) 100 mm water level and (**c**) 150 mm water level.

Figure 13 shows the p–s curve at the upper right corner point of the model, the location of the midpoint of the loading plate. The analysis of the figure shows that, with the increasing height of the water level, the bearing capacity of the foundation has a significant decrease. The bearing capacity of the foundation drops from 378.7 kPa to 335.2 kPa as the water level rises from 0 mm to 50 mm. There is a decrease of 11.5%. When the water level rises from 50 mm to 100 mm, the bearing capacity of the foundation drops from 336.8 kPa to 281.4 kPa. There is a decrease of 16.4%. When the water level rises from 100 mm to 150 mm, the bearing capacity of foundation decreases from 281.4 kPa to 191.2 kPa; the rate of decrease is 32.1%. This means that the submerging effect of the water level on the foundation obviously reduces the bearing capacity of the foundation, and the rate of decrease increases with the increase in the water level. This is basically consistent with the conclusion drawn from the test.
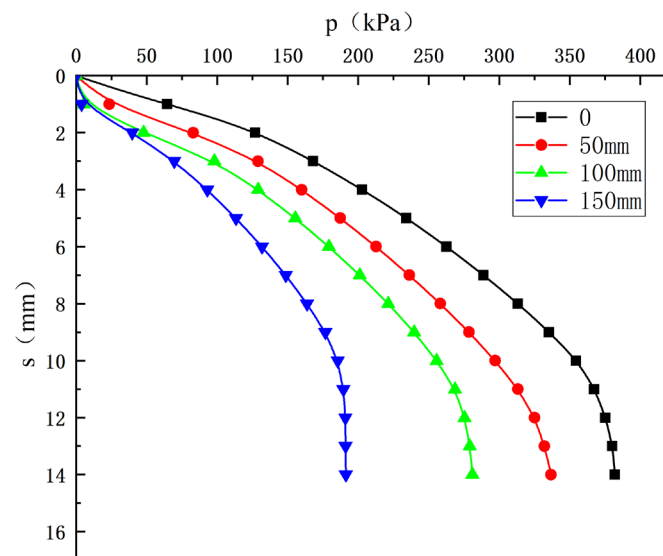
Figure 13. The p–s curves for different water-level heights.

3.5. Discussion

In this study, a novel test device was designed that can simulate the effect of the groundwater level on the foundation bearing capacity. This opens up a new idea for the indoor model test of foundation bearing capacity. In addition, a new idea of numerical simulation was proposed. The problem was simplified by dividing the ground affected by groundwater harvesting into three sections with different soil saturation levels. Compared with the traditional foundation-bearing-capacity theory, this model has the advantage of considering the influence of the water-level fluctuation. In other theories, the water line is usually represented as a straight line. This is not accurate, because the soil capillary effect can make the water level uneven. The water line may not be static, after all. Fluctuating water levels are also common. Based on this, the formula was improved. A new expression form of pore water pressure was derived for sinusoidal fluctuation. The effective stress of the foundation soil was also changed.

The simulation results were compared with the experimental results to verify the reliability of the conclusion. The error between the simulation calculation and the test is within the acceptable range. This proves the feasibility of the simulation method. Other scholars have studied the mechanical properties of unsaturated soil and found that its cohesion and internal-friction angle decrease with the increase in soil water content [30]. This is consistent with the conclusion of this paper. The reliability of the experiment and numerical simulation was verified by internal and external verification. This makes it possible to raise the groundwater-level warning in practical engineering

The experiment had some limitations. As the bottom of the model box is impervious to water, the bottom of the foundation was regarded as an impervious layer in this experiment and simulation. In fact, the bottom of the model box is connected to the pump, so it cannot be considered impervious. In addition, the capillary effect makes it difficult to distinguish the water level of the foundation soil, so there are errors.

This numerical simulation also has some limitations. First, the load-transfer mode and foundation-failure mode of deep foundation are quite different from those of a shallow foundation, so this model cannot be directly applied to a deep foundation. Second, the accuracy of the model in other types of foundation soil cannot be guaranteed, due to the differences in the water absorption and permeability of different types of soil.

4. Conclusions

In this study, the influence of water-level change on the bearing capacity of shallow foundation was studied by combining a model test and numerical simulation. The major conclusions are summarized as follows:

1.　The height of water level and the frequency of water-level fluctuation are negatively correlated with the bearing capacity of the foundation, and the relationship of change is nonlinear. The water-level fluctuation can strengthen the capillary effect and expand the range of saturated soil in the foundation.

2.　In this study, the influence of the water-level fluctuation was added to the traditional calculation of the foundation bearing capacity. A new expression form of pore water pressure was derived for sinusoidal fluctuation. The average error between the calculated bearing capacity and the test results is less than 8%. It shows that this theory can be used to calculate the bearing capacity of a foundation under water-level fluctuation.

3.　This model can well predict the change in the foundation bearing capacity due to the water-level change. It has a good early warning function for an engineered foundation that has been under a high groundwater level for a long time.

4.　This model also has some limitations. It is currently only applicable to sandy shallow foundations. In the future, the model will be expanded to apply to more types of foundations.

References

1.　Ge, S.P.; Yao, X.J. Response characteristics of pore pressure in soils nearby metro tunnel due to train vibration loading. *J. Eng. Geol.* **2015**, *23*, 1093–1099. [CrossRef]

2.　Yan, C.B.; Zhang, Y.C.; Chen, Y.G. Slip analysis of silted interbedded slope considering cumulative damage effect of blasting. *Hydr. Sci. Eng.* **2020**, *1*, 104–113. [CrossRef]

3.　Xu, D.S.; Huang, M.; Zhou, Y. One-dimensional compression behavior of calcareous sand and marine clay mixtures. *Int. J. Geom.* **2020**, *20*, 04020137. [CrossRef]

4.　Shi, Y.J.; Yan, X.X.; Chen, D.P. Engineering geological structure establishment and conditions assessment integrating land and sea in Shanghai coastal area. *Hydrogeol. Eng. Geol.* **2017**, *44*, 96–101. [CrossRef]

5.　Wang, W.D.; Wei, J.B.; Wu, J.B.; Zhou, R.F. Field test and analysis on effects of pile driving with high-frequency and resonance-free technology on surrounding soil. *J. Build. Struct.* **2020**, *42*, 132–138. [CrossRef]

6.　Wang, J.N.; Zhuang, H.Y. Shaking table test on liquefaction characteristics of foundation around a complicated subway station with diaphragm walls. *Chin. J. Geotech. Eng.* **2020**, *42*, 1859–1866. [CrossRef]

7.　Xu, D.S.; Liu, H.B.; Rui, R.; Gao, Y. Cyclic and postcyclic simple shear behavior of binary sand-gravel mixtures with various gravel contents. *Soil Dyn. Earth Eng.* **2019**, *123*, 230–241. [CrossRef]

8.　Xu, D.S.; Liu, Q.C.; Qin, Y.; Chen, B. Analytical approach for crack identification of glass fiber reinforced polymer–sea sand concrete composite structures based on strain dissipations. *Struct. Health Monit.* **2021**, *20*, 2778–2790. [CrossRef]

9.　Hu, Y.Q.; Hong, C.Y.; Zhang, Y.F.; Ling, G.W. A monitoring and warning system for expressway slopes using FBG sensing technology. *Int. J. Distr. Sens. Netw.* **2018**, *14*, 1–12. [CrossRef]

10.　Terzaghi, K. Arching in Ideal Soils. In *Theoretical Soil Mechanics*; Wiley: New York, NY, USA, 1943.

11.　Hansen, J.B. *A General Formula for Bearing Capacity*; Danish Geotechnical Institute: Copenhagen, Denmark, 1961.

12.　Khalid, M.; Sardar, A.; Jaffar, S. Influence of Footing Shapes and GWT on Bearing Capacity and Settlement of Cohesive Soil Beneath Shallow Foundations. *Nucleus* **2020**, *57*, 39–48.

13.　Boushehrian, J.H.; Hataf, N. Experimental and numerical investigation of the bearing capacity of model circular and ring footings on reinforced sand. *Geo. Geom.* **2003**, *21*, 241–256. [CrossRef]

14. Dixit, M.; Patil, K. Effect of Depth of Footing and Water Table on Bearing Capacity of Soil. In Proceedings of the Indian Geotechnical Conference, Mumbai, India, 16–18 December 2010.

15. Shu, B.; Chen, S.; Lu, J.F. Analysis of fluid–solid coupling mechanical behaviour of non-linear for soft clay foundation. *Mater. Res. Innov.* **2015**, *19*, 727–732. [CrossRef]

16. Yao, P.F.; Qi, S.W.; Zhang, M. Simplified method for determining shear strength of unsaturated soils based on different paths. *Rock Soil Mech.* **2009**, *9*, 2605–2608. [CrossRef]

17. Pei, H.F.; Zhang, S.Q.; Borana, L.; Zhao, Y.; Yin, J.H. Slope stability analysis based on real-time displacement measurements. *Measurement* **2019**, *131*, 686–693. [CrossRef]

18. Kassem, M.; Soliman, A.; Naggar, H. Sustainable approach for recycling treated oil sand waste in concrete: Engineering properties and potential applications. *J. Clean. Prod.* **2018**, *204*, 50–59. [CrossRef]

19. Xu, D.S.; Yin, J.H.; Liu, H.B. A new measurement approach for deflection monitoring of large-scale bored piles using distributed fiber sensing technology. *Measurement* **2018**, *117*, 444–454. [CrossRef]

20. Yao, P.F. Discussion on shear strength of unsaturated soils. *Rock Soil Mech.* **2009**, *30*, 2315–2318. [CrossRef]

21. Cai, G.Q.; Zhang, C.; Li, J. Study on prediction method of swcc considering initial dry density. *Chin. J. Geotech. Eng.* **2018**, *40*, 27–31. [CrossRef]

22. Xu, D.S.; Zhu, F.B.; Lalit, B.; Fan, X.C.; Liu, Q.B. Construction solid waste landfills: Risk assessment and monitoring by fibre optic sensing technique. *Geomat. Nat. Hazard Risk* **2021**, *12*, 63–83. [CrossRef]

23. Wen, B.P.; Hu, Y.Q. Effece of particle size distribution on the metric suction of unsaturated clayey soils. *Hydrogeol. Eng. Geol.* **2008**, *6*, 50–55. [CrossRef]

24. You, R.Z.; Ren, L.; Song, G.B. A novel fiber Bragg grating (FBG) soil strain sensor. *Measurement* **2019**, *139*, 85–91. [CrossRef]

25. Qin, Y.; Wang, Q.K.; Xu, D.S.; Yan, J.M.; Zhang, S.S. A FBG based earth and water pressure transducer with 3D fused deposition modeling approach for soil mass. *J. Rock Mech. Geotech.* **2022**, *14*, 663–669. [CrossRef]

26. Xu, D.S.; Chen, W.; Fan, X.C. Experimental investigation of particle size effect on the self-healing performance of microcapsule for cemented coral sand. *Constr. Build. Mater.* **2020**, *256*, 119343. [CrossRef]

27. Zhu, H.H.; Shi, B.; Yan, J.F.; Zhang, J.; Wang, J. Investigation of the evolutionary process of a reinforced model slope using a fiber-optic monitoring network. *Eng. Geol.* **2015**, *186*, 34–43. [CrossRef]

28. Huang, K.; Wan, J.W.; Chen, G.; Zeng, Y. Testing study of relationship between water content and shear strength of unsaturated soils. *Rock. Soil Mech.* **2012**, *33*, 2600–2604. [CrossRef]

29. Su, L.J.; Zhang, Y.J.; Wang, T.X. Investigation on permeability of sands with different particle sizes. *Rock Soil Mech.* **2014**, *35*, 1289–1294. [CrossRef]

30. Wang, D.L.; Luan, M.T.; Yang, Q. Experimental study of soil-water characteristic curve of remolded unsaturated clay. *Rock Soil Mech.* **2009**, *30*, 751–756. [CrossRef]

31. Ma, S.K.; Huang, M.S.; Fan, Q.Y. Unsaturated soil strength theory based on total stress strength indexes of saturated soil and its application. *Chin. J. Geotech. Eng.* **2009**, *28*, 635–640. [CrossRef]

32. Tang, L.S. New suggestion on shear strength in unsaturated soil based on suction between grains. *Chin. J. Geotech. Eng.* **2001**, *23*, 412–417. [CrossRef]

33. Huang, M.S.; Qu, X.; Lu, X.L. Regularized finite element modeling of progressive failure in soils within nonlocal softening plasticity. *Comput. Mech.* **2017**, *62*, 347–358. [CrossRef]

34. Forest, S. Micromorphic approach for gradient elasticity, viscoplasticity and damage. *J. Eng. Mech.* **2009**, *135*, 117–131. [CrossRef]

35. Lu, X.L.; Xue, D.W.; Huang, M.S. A shear hardening plasticity model with nonlinear shear strength criterion for municipal solid waste. *Comput. Geotech.* **2018**, *104*, 204–215. [CrossRef]

36. Lin, H.Z.; Li, G.X.; Yu, Y.Z. Influence of matric suction on shear strength behavior of unsaturated soils. *Rock Soil Mech.* **2007**, *28*, 1931–1936. [CrossRef]

37. Lee, J.K.; Jeong, S. Undrained bearing capacity factors for ring footings in heterogeneous soil. *Comput. Geotech.* **2016**, *75*, 103–111. [CrossRef]

38. Shen, J.H.; Xu, D.S.; Liu, Z.W.; Wei, H.Z. Effect of particle characteristics stress on the mechanical properties of cement mortar with coral sand. *Constr. Build. Mater.* **2020**, *260*, 119836. [CrossRef]